



Article

Origin of the Shangfang Tungsten Deposit in the Fujian Province of Southeast China: Evidence from Scheelite Sm–Nd Geochronology, H–O Isotopes and Fluid Inclusions Studies

Lü-Yun Zhu ^{1,2,*} , Shao-Yong Jiang ^{1,*}, Run-Sheng Chen ² and Ying Ma ¹ 

¹ State Key Laboratory of Geological Processes and Mineral Resources, School of Earth Resource, Collaborative Innovation Center for Exploration of Strategic Mineral Resources, China University of Geosciences, Wuhan 430074, China; maying9607@gmail.com

² Fujian Institute of Geological Survey and Research, Fuzhou 350013, China; crs2008@126.com

* Correspondence: zhulvyun@126.com (L.-Y.Z.); shyjiang@cug.edu.cn (S.-Y.J.); Tel.: +86-027-678-835-05 (S.-Y.J.)

Received: 29 September 2019; Accepted: 16 November 2019; Published: 19 November 2019



Abstract: The Shangfang deposit is a recently discovered large-scale tungsten deposit (66,500 t at 0.23% WO₃), which is located near the western boundary of the Southeastern Coastal Metallogenic Belt (i.e., Zhenghe–Dafu fault), and adjacent to the northeast of the Nanling Range Metallogenic Belt. Unlike many other W–Sn deposits in this region that occur within or near the granites, the orebodies in the Shangfang deposit all occur within the amphibolite of Palaeoproterozoic Dajinshan Formation and have no direct contact to the granite. In this study, we carry out a thermal ionization mass spectrometer (TIMS) Sm–Nd isotope analysis for the scheelites from the orebody, which yields a Sm–Nd isochron age of 157.9 ± 6.7 Ma (MSWD = 0.96). This age is in good agreement with the previously published zircon U–Pb age (158.8 ± 1.6 Ma) for the granite and the molybdenite Re–Os age (158.1 ± 5.4 Ma) in the deposit. Previous studies demonstrated that the W–Sn deposits occurring between Southeastern Nanling Range and Coastal Metallogenic Belt mainly formed in the two periods of 160–150 Ma and 140–135 Ma, respectively. The microthermometry results of fluid inclusions in scheelite and quartz are suggestive of a near-isothermal (possibly poly-baric) mixing between two fluids of differing salinities. The H–O isotope results illustrate that the ore-forming fluids are derived from magma and might be equilibrated with metamorphic rocks at high temperature. The Jurassic granite pluton should play a critical role for the large hydrothermal system producing the Shangfang W deposit. Furthermore, the negative $\epsilon_{\text{Nd}}(t)$ of −14.6 obtained in the Shangfang scheelite suggests for the involvement of the deep crustal materials. In general, subduction of the paleo-Pacific plate caused an extensional tectonic setting with formation of the Shangfang granites and related W mineralization, the geological background of which is similar to other W deposits in the Nanling Range Metallogenic Belt.

Keywords: Sm–Nd age of scheelite; fluid inclusion; H–O isotope; Shangfang tungsten deposit

1. Introduction

Tungsten (W) is a critical metal that has been widely used for the new industrial products (e.g., filaments, electrodes, projectiles, catalysts). According to the statistics of the U.S. Geological Survey, China is the most crucial producer of W in the world at present [1]. As one of the dominant mineral resources, most of the W deposits are found in three metallogenic belts in South China (i.e., the Nanling Range, Southeastern Coast, and Jiangnan Orogen). All of these large-scale mineral systems in South China are genetically related to the Mesozoic granites but with different mineralogical

epochs. The W–Sn deposits in the Nanling Range Metallogenic Belt, mainly comprising skarn and wolframite–quartz vein types, display ages clustering in the 160–150 Ma range [2–4]. Recently several granite-related large-scale W–Cu and W–Mo deposits (WO_3 : more than 5.0 million tons) have been discovered in the Jiangnan Orogen, which is located in the southeast margin of Yangtze Craton, and to the south part of Middle–Lower Yangtze River Valley. Several dating results have demonstrated that 150–130 Ma is the main mineralization epoch for these newly discovered world-class tungsten deposits (e.g., Dahutang), in which the W ore mostly occurs as veinlet or dissemination in granite and granite-granodiorite porphyries [5,6]. The Southeastern Coastal Metallogenic Belt is located at the continental margin of Eurasia, and is adjacent to the southeast of the Nanling Range Metallogenic Belt. In contrast with the Nanling Range Metallogenic Belt, the W–Sn deposits of the Southeastern Coastal Metallogenic Belt are concentrated in the eastern Guangdong Province. The W–Sn mineralization styles are mainly associated with volcanic–subvolcanic rocks, and the ages of which are in the range of 145–135 Ma [7].

The Shangfang W deposit is located near the Zhenghe–Dafu fault that is regarded as the western boundary of Southeastern Coastal Metallogenic Belt, and adjacent to the northeast of the Nanling Range Metallogenic Belt. The age of this recently found deposit is still not fully constrained, hindering its linking with the known metallogenic events in South China. Previously, Chen, et al. [8] reported a zircon U–Pb age of granite (158.8 ± 1.6 Ma) and a molybdenite Re–Os age (158.1 ± 5.4 Ma) for the deposit. Because the ore bodies of the Shangfang W deposit all occur in the amphibolite of Palaeoproterozoic Dajinshan Formation that does not have direct contact with the granite, it is a risk to predict the mineralization age of this deposit only by the zircon U–Pb age of granite. Meanwhile, the molybdenite Re–Os age may only represent the age of Mo mineralization, not the W mineralization since the Mo and W orebodies are separated in the deposit. In contrast, the Sm–Nd isochron age of scheelite can provide direct evidence on the tungsten mineralization age. Consequently, the first aim of the present work is to ascertain the W mineralization age by dating the scheelite. A second aim is to better constrain the origin of the ore-forming fluids and the mineralizing conditions, combining information from geology, petrography, fluid inclusion, and stable isotope (H–O) studies. Finally, we address the understanding of the large-scale mineral systems in South China during the Mesozoic.

2. Regional Geology

The South China Block is located at the eastern margin of the Eurasian plate and surrounded by the Qinling–Dabie–Sulu orogenic belt, the Tibetan Block and the Indochina Block (Figure 1a). Generally, the amalgamation of the Yangtze Block (to the northwest) and the Cathaysia Block (to the southeast) formed the South China Block along the Jiangshan–Shaoxing fault during the Neoproterozoic [9,10]. The Yangtze and Cathaysia blocks have distinctive Precambrian basements and different tectonic evolution histories [10–13]. The basement of the Yangtze Block consisting of Proterozoic rock with a rare Archean outcrop [13–16]. In contrast, the Cathaysia Block is composed predominantly of Paleoproterozoic outcrop while certainly preserving the Archean basement in the lower crust. The Neoproterozoic (the Sinian) formation is in unconformable contact with the Paleoproterozoic basement that also regarded as the probable source of W deposits in the Cathaysia Block [17,18]. In the South China Block, there is the succession of three major tectonic–magmatic events (Kwanghsian, Indo-Sinian, Yanshanian), all of which are associated with the rare metal endowment. As shown in Figure 1b, both the Yangtze and Cathaysia blocks are large igneous provinces during the Yanshanian, because of the three stages of lithospheric extensions ranging respectively from 170–150 Ma, 140–126 Ma, and 110–80 Ma [3,4]. All the peaks of granite magmatism coeval with three bursts of Sn–W, which formed three large-scale metallogenic provinces, named the Southeastern Coastal Metallogenic Belt, Nanling Region, and the Jiangnan Orogen. And these metallogenic provinces reserve the mass large W deposits of the South China Block [3,5,6,19–21].

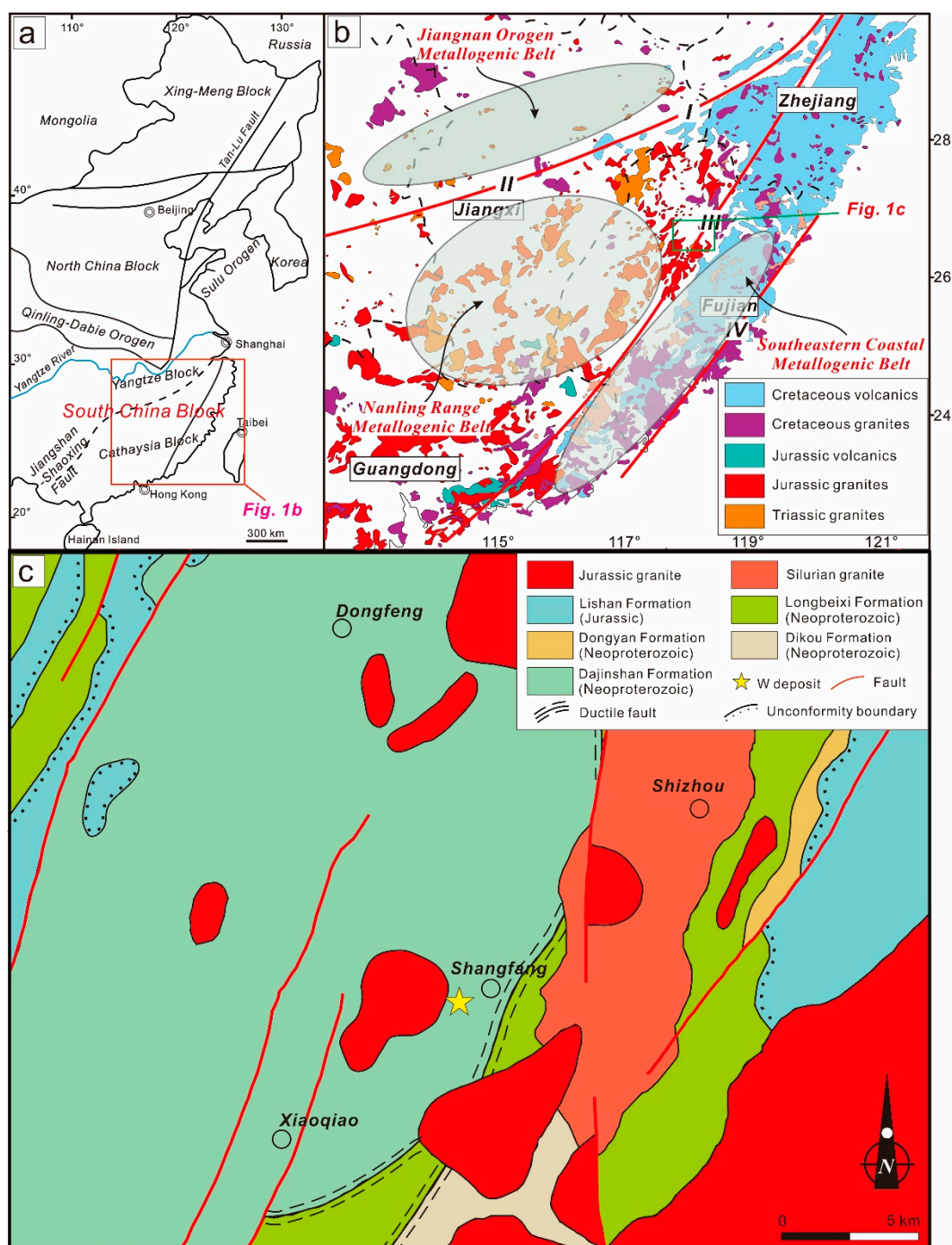


Figure 1. (a) Tectonic scheme of eastern China; (b) schematic map of SE China showing the distribution of the Mesozoic granitic and volcanic rocks (modified from Zhou et al. [22]); (c) geological map of the Dongfeng-Xiaoqiao region showing the location of the Shangfang W deposits. I—Jiangshan-Shaoxing fault; II—Pingxiang-Yushan fault; III—Zhenghe-Dapu fault; IV—Changle-Nan’ao fault.

Not only the spatial and temporal distribution, but also the type of granite displays a series of variation due to the transition of the Pacific plate subduction [22–24]. In the South China Block, the Indosinian granites are predominantly composed of S-type granites with minor calc-alkaline I-type granites, but few of coeval volcanic rocks [22,25–28]. In contrast, the Yanshanian granites are characterized by dominant I-type granites associating with coeval volcanic rocks, but fewer S- and A-type granites. The Early Yanshanian (Jurassic) granites are mainly distributed in the interior

of the South China Block and associated with minor coeval volcanic rocks, whereas both granites and massive felsic volcanic rocks are concentrated in the coastal region of the South China Block during the Late Yanshanian (Cretaceous) [23,29,30]. Some researchers proposed that there was an oceanward-younger migration trend for Mesozoic magmatism in the South China Block especially during the Late Mesozoic [22,27,31,32].

3. Geology of the Shangfang W Deposit

3.1. Local Geology

The Shangfang W deposit (26°58'45" to 27°02'45" N, 118°31'00" to 118°35'15" E) is situated about 25 km east of Jian'ou City and covers an area of ~39 km² (Figure 1c). The local geology of the Shangfang deposit is mostly represented by the Paleoproterozoic Dajinshan Formation and the Jurassic granitic rocks. The Paleoproterozoic Dajinshan Formation (1.90 to 1.86 Ga) is mainly composed of amphibolite to granulite facies sillimanite–garnet–kyanite schist, fine-grained leucogneiss, and amphibolite (Figures 2 and 3) [33,34]. According to previous research, amphibolite to granulite facies metamorphism peaked during the Early Paleozoic, and the metamorphic temperature and pressure conditions were 570–680 °C and 4.3–7.0 kbar [35], or 590–625 °C and 4.2–4.5 kbar [36]. In the mining area, the amphibolite is the main host rock of the orebodies. The amphibolite contains amphibole (40%–65%), plagioclase (30%–45%) with accessory magnetite, zircon, apatite, and titanite, and displays as massive or thick-bedded (Figure 3a). The Paleoproterozoic basement rocks have been intruded by several phases of Jurassic granitic rocks including biotite syenogranite (Figure 3b) and granite porphyry dykes. The biotite syenogranite occurs both at the outcrops and at various underground levels (Figure 2). These rocks consist of K-feldspar (30%–40%), plagioclase (20%–30%), quartz (20%–30%), and minor biotite (~5%). Chen et al. have reported zircon U–Pb dating results by laser ablation inductively coupled plasma mass spectrometry (LA-ICP–MS) and suggested the biotite syenogranite emplaced at 158.8 ± 1.6 Ma [8]. The biotite syenogranite has high contents of SiO₂ (74.82%–76.81%) and alkalis (K₂O + Na₂O = 7.78–8.94%), with K₂O/Na₂O and A/CNK values of 1.39–2.07, 1.01–1.05, respectively, and as such belongs to the high-K calcic–alkaline series. It is enriched in light rare earth elements (LREEs) and depleted in high field strength elements (HFSEs). Based on the geochemical characteristics of the granite, they suggested that the Shangfang biotite syenogranite was produced mainly by partial melting of the lower crustal materials with only small contributions from the mantle components [8]. Furthermore, the biotite syenogranite has a genetic relationship with tungsten mineralization and associated hydrothermal alterations, although few granite bodies are in contact with the ore bodies. Structurally, the mining area is characterized by the NE-trending syncline and some younger NW-, and N–S-trending faults. The NE-trending faults controlled not only the emplacement of the granite porphyry dykes but also the distribution of Shangfang orebodies.

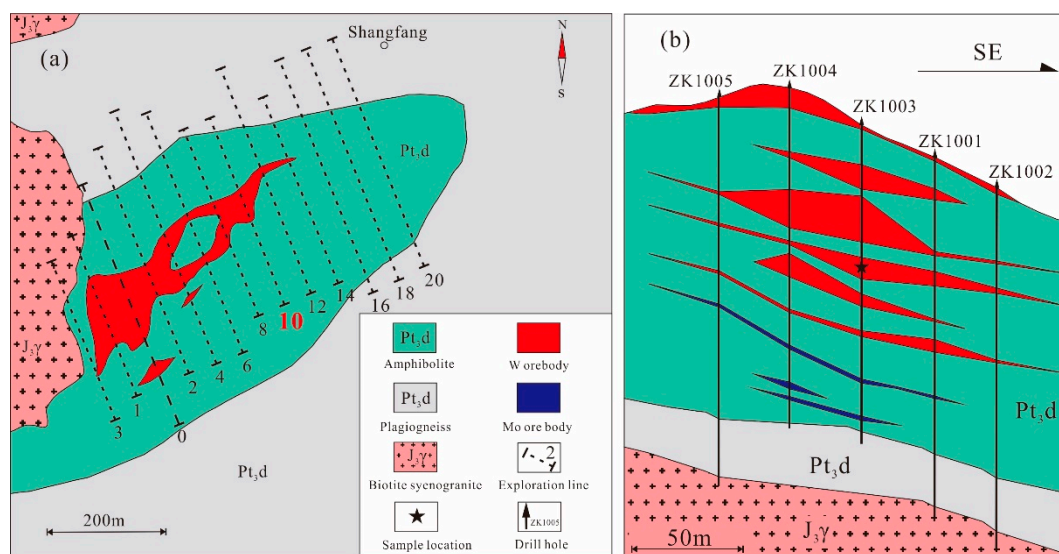


Figure 2. The geologic map (a), and representative cross-section of No.10 exploration line (b) of the Shangfang W deposit, showing distribution and morphology of the W and Mo orebodies.

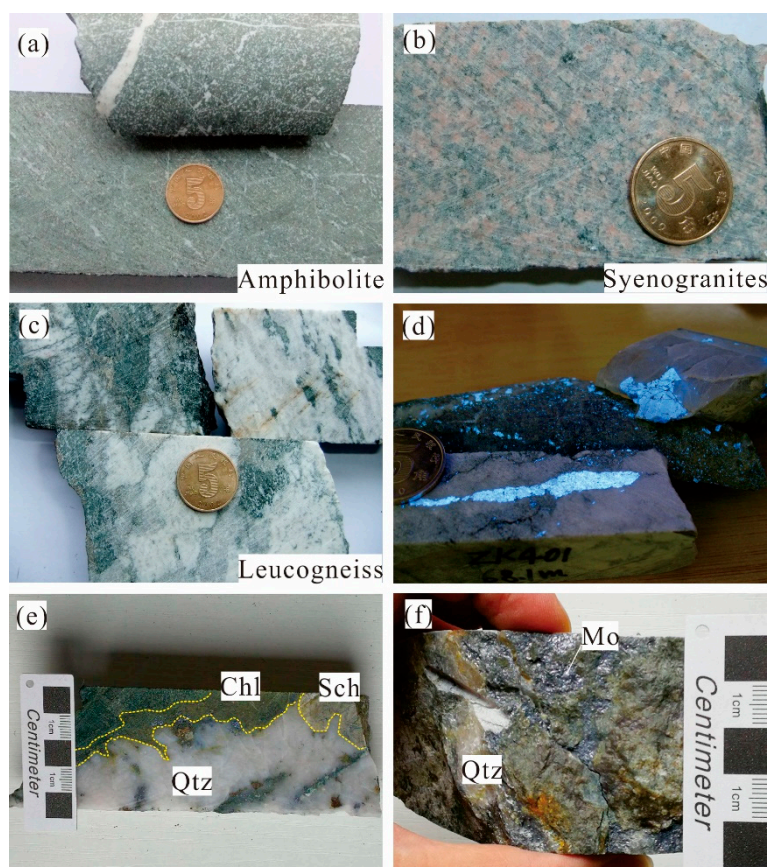


Figure 3. Representative photographs of rock, hydrothermal alteration, and mineralization features in the Shangfang W deposit. (a) amphibolite; (b) biotite syenogranite; (c) leucogneiss; (d) photographs under ultraviolet light showing massive and disseminated scheelite; (e) syn-ore scheelite–quartz veinlets within the chlorite-altered amphibolite; (f) molybdenite along cleavage of quartz veinlet. Abbreviations: Qtz = quartz; Sch = scheelite; Chl = Chlorite; Mo = molybdenite.

3.2. Mineralization

The W mineralization at Shangfang generally occurs as vein, veinlet, and dissemination in the hydrothermally altered amphibolites of the Paleoproterozoic Dajinshan Formation. The Shangfang W deposit consists of nine main ore bodies and contains an estimated resource of 66,500 t of WO_3 at an average grade of 0.23% (Table 1), according to prospecting report from Fujian Institute of Geological Survey and Research. The ore body shows either a lens-shape or a tubular-shape in paralleled distribution (Figure 2b). The mineralization of the Shangfang deposit is aligned along with a NE–SW trend, with a maximum length of 800 m, and a width of up to 300 m. The W and Mo mineralization in the Shangfang deposit displays zoning which is characterized by upper scheelite ore bodies and lower molybdenite ore bodies (Figure 2b). The ore minerals within various veins consist mainly of scheelite, pyrrhotite, pyrite, chalcopyrite, and molybdenite, with minor galena and sphalerite, and these minerals are generally enriched in the quartz–scheelite veins. The massive or disseminated scheelite usually occur in the quartz veins or amphibolite as tetragonal dipyramidal crystals with a grain size range from 0.1 to 30 mm (Figure 3d). Major gangue minerals are quartz, chlorite, and actinolite for quartz-vein-type ores (Figure 3e). The amount of W ore is far more than that of Mo ore that only occurs as the molybdenite along some quartz veinlet (Figure 3f). Among the 20 exploration lines, only several ones found Mo orebody in a small amount.

Table 1. Summary of main orebody characteristics in the Shangfang W deposit.

Orebody Number	Size (m)			Average Grade	Spatial
	Length	Width	Thickness	WO_3 (%)	Attitude
No.1	800	300	4.3	0.271	Paralleled distribution
No.2	600	200	4.27	0.123	
No.3	400	250	7.23	0.187	
No.4	400	200	7.88	0.245	
No.5	400	250	1.63	0.152	
No.6	800	200	9.65	0.311	
No.7	400	120	1.64	0.392	
No.8	400	120	6.98	0.203	
No.9	400	120	3.92	0.154	

3.3. Alteration

The emplacement of the Shangfang biotite syenogranite resulted in the hydrothermal alteration of the amphibolite of the Paleoproterozoic Dajinshan Formation in a zone of several hundred meters wide (Figure 2). As shown in Figure 3d,e, the quartz vein cuts the amphibolite and produces clear alteration zones containing scheelite. The disseminated scheelite in the alternation zones could be interpreted as syngenetic hydrothermal mineralization, possibly related to the chemical element exchange between the hydrothermal quartz vein and amphibolite (Figure 3e).

In the Shangfang deposit, the most intensive hydrothermal alteration occurring in and around the mineralized quartz vein. The key components of alteration assemblages are actinolite, chlorite, sericite, and quartz. Actinolitization and silicification are the most widespread alteration type in the deposit. The diopside and tremolite might be the product of hydrothermal alteration in the early stage (Figure 4a). Due to the following hydrothermal alteration, the diopside was altered to actinolite (Figure 4b), which coexisted with the early-stage scheelite (Figure 4c). Silicification posterior to actinolitization, and coexisted with chloritization and phyllic alteration that may overprint early alteration in wall rock (Figure 4d). Sericite commonly replaced plagioclase in biotite syenogranite (Figure 4e). Most of the chlorite formed by replacement of the amphibole in the amphibolite (Figure 4f). In the mineralized quartz vein, the scheelite commonly coexists with massive pyrrhotite, minor chalcopyrite and molybdenite (Figure 4g,h). The final stage of hydrothermal alteration was carbonatization, which overprinted all previous alteration types and usually coexisted with fluorite

and along fractures (Figure 4i). According to the field and petrographic relations, the paragenetic sequence of gangue and ore minerals in the Shangfang W deposit is shown in Figure 5.

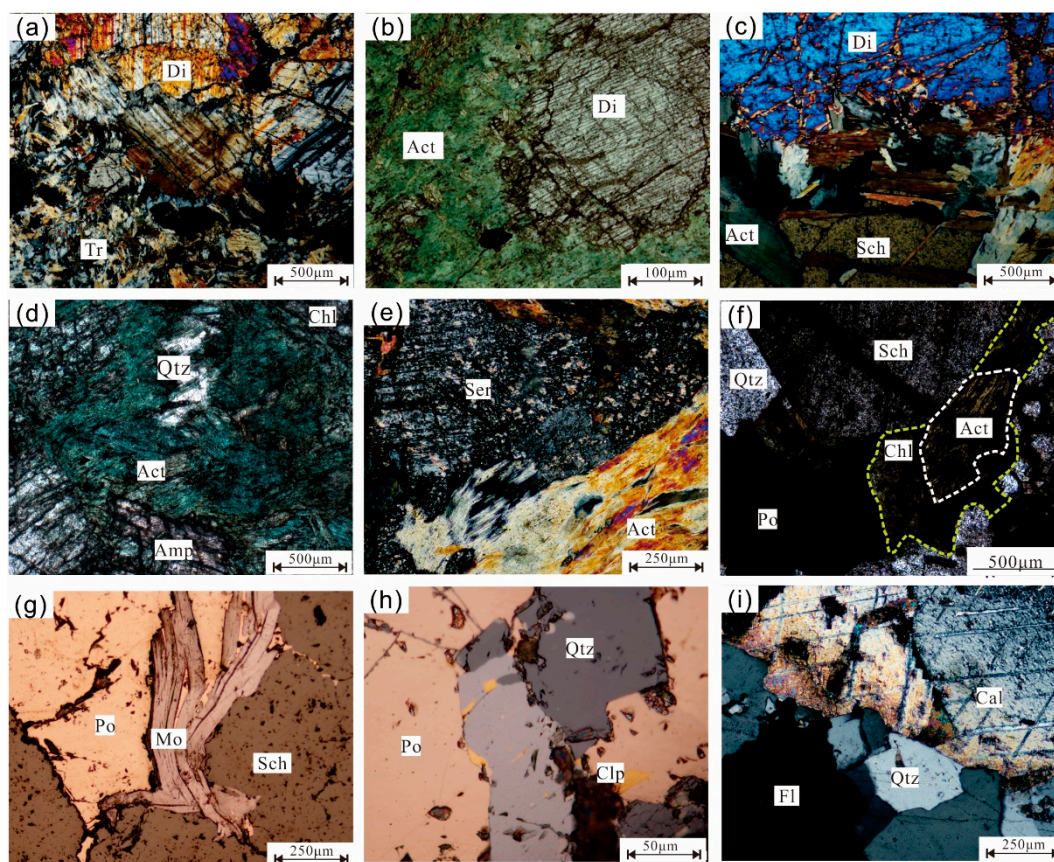


Figure 4. Reflected- and transmitted-light photomicrographs showing the typical morphology and textures of ore and gangue minerals in the Shangfang W deposit. (a) diopside and tremolite coexist in the early stage; (b) the diopside was altered to actinolite; (c) actinolite coexists with the early-stage scheelite; (d) chloritization and silicification; (e) Sericite alternated from plagioclase; (f) chlorite alternated from amphibole; (g,h) the scheelite coexists with massive pyrrhotite, chalcopyrite and minor molybdenite; (i) calcite and fluorite. Abbreviations: Di = Diopside; Tr = Tremolite; Act = Actinolite; Sch = Scheelite; Qtz = quartz; Ser = sericite; Po = Pyrrhotite; Chl = Chlorite; Mo = molybdenite; Clp = Chalcopyrite; Cal = calcite; Fl = fluorite.

4. Analytical Methods

4.1. Fluid Inclusion Measurement

A Nikon Eclipse LV100POL microscope was adopted for the fluid inclusion petrographic study at the National Demonstration Center for Experimental Mineral Exploration Education of the China University of Geosciences (Wuhan). Liquid N₂ flow was used for cooling down. Fluid inclusions were carefully observed to identify their forms and spatial distributions. A Linkham THMS-600 heating-freezing stage (−196 to 600 °C) was used for microthermometric measurements at the Collaborative Innovation Center for Exploration of Strategic Mineral Resources. This stage was calibrated with delicate fluid inclusions of pure H₂O (ice melting temperature = 0), critical temperature = 371.4 °C) and pure CO₂ (CO₂ melting temperature = −56.6 °C). The precisions of temperatures are respectively about ± 0.5 °C, ± 0.2 °C, and ± 2 °C for the variation range of −120 and −70 °C, −70 to 100 °C and more than 100 °C. The high heating-freezing rate of 1–10 °C/min was adopted for the early stage, but a lower rate of 0.1–1 °C/min to closing phase transformation.

In other words, ice melting temperatures and homogenization temperatures were respectively obtained under a rate of 0.1 °C and 1 °C. The freezing temperature was collected before heating temperature during microthermometric measurement. According to the types of fluid inclusions, we examined and recorded the final melting temperature (T_{m-ice}) and total homogenization temperature (T_h).

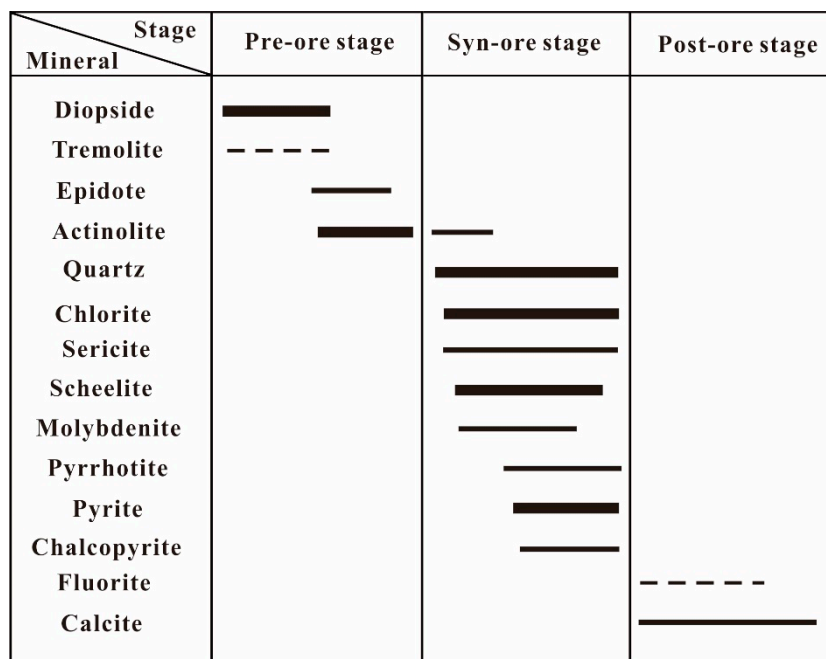


Figure 5. The paragenetic sequence of gangue and ore minerals in the Shangfang W deposit. Line thickness represents the relative amount of minerals.

4.2. Hydrogen and Oxygen Isotopic Analysis

The measurements of H–O isotopic composition were carried out by a Finnigan MAT253 mass spectrometer in the analytical Laboratory of Beijing Research Institute of Uranium Geology, Beijing, China. The fluid inclusions in quartz separates were broken for extracting the water in them. By the reaction with heated chromium, the water would release hydrogen for isotopic measurement. The oxygen isotopic analysis of quartz was performed by the conventional BrF_5 method by Clayton and Mayeda [37]. All the results of H–O isotopic composition were calibration against the V-SMOW (Vienna standard mean ocean water) with analytical errors of $\pm 2\%$ for δD and $\pm 0.2\%$ for $\delta^{18}O$.

4.3. Scheelite Sm-Nd Isotope Dating

In this study, we use the standard heavy liquid method to separate scheelite from other silicate minerals in the ore samples. Under a UV lamp, the scheelite grains were further selected and purified by handpicking under a binocular microscope. The pure scheelite was powdered in an agate mortar before sample dissolution. In general, the procedure of scheelite dissolution is modified from the method suggested by Chu, et al. [38]. At first, 30 to 50 mg samples were dissolved by a mixture acid of 2 mL HF (22 M) + 1 mL HNO_3 (15 M) + 0.2 mL concentrated $HClO_4$ in steel jacketed Teflon digestion vessels. All the vessels were placed and heated in an oven at 190 °C over three days. After firstly drying down on a hot plated at 150 °C, the sample residues in vessels were leached by 4 mL HCl (6 M) back to a solution that was evaporated to dryness subsequently. Then, 1 mL HCl (2.5 M) was used to leach the sample residues again, before another process of steel-jacketed Teflon digestion at 150 °C over 24 h. Finally, the sample solution was centrifuged, and the supernatant was pipetted out as completely as possible for column chemistry separation. Isotopic ratio measurements were made on a thermal ionization mass spectrometer (TIMS) at the Wuhan Institute of Geology and Mineral Resources, China.

The mass fractionation of Nd isotope ratio was calibrated against a natural $^{146}\text{Nd}/^{144}\text{Nd}$ ratio of 0.7219. The reproducibility of the isotopic ratios is about 0.003% at the two-sigma level, and the precision for the Nd and Sm concentrations is about $\pm 0.5\%$ of the quoted values at the two-sigma level.

5. Results

5.1. Fluid Inclusion

5.1.1. Petrography and Types of Fluid Inclusions

Due to weathering of the outcrop, all the samples were collected from drill cores of the Shangfang deposit for the fluid inclusion studies. To establish the overall fluid evolution history of the study area, we examine fluid inclusions of major transparent minerals, including scheelite, quartz, and calcite (Figure 6). According to the distribution characters of primary and secondary fluid inclusions, the clustered inclusions and randomly distributed isolated fluid inclusions in crystals of scheelite, quartz, and calcite can be interpreted as the primary one in origin. Whereas those displaying linearly along microfractures of transgranular trails should be the secondary fluid inclusions. All the fluid inclusions observed at room temperature and classified on the basis of the phase relationships. Four main types of fluid inclusions were recognized: (i) monophasic vapor (V) inclusions (Figure 6a); (ii) aqueous liquid (L-V) inclusions (Figure 6b,c), which can homogenize to liquid upon heating (i.e. generally ~60 to 80 vol. %); (iii) vapor-rich aqueous (V-L) inclusions (Figure 6d–f), which can be heated to homogenise vapor (i.e., typically >60 vol. % vapor); (iv) liquid aqueous (L) inclusions (Figure 6g–i). The V inclusions are rare and can be only observed in the scheelite. The number of V-L inclusions is also limited, but they are distributing in scheelite and quartz. Both L and L-V inclusions are common and observed among scheelite, quartz, and calcite. The primary L-V inclusions are adopted for microthermometry study.

5.1.2. Microthermometry Results

Due to few primary fluid inclusions found in transparent minerals of the pre-ore stage, the scheelite-quartz and calcite were respectively measured for homogenization temperatures and salinities of fluid inclusions for syn-ore and post-ore stage. Most of the fluid inclusions of each stage contain a liquid and vapor phase (Figure 6f–h). However, it can still be found that several inclusions only consisted of liquid or vapor phase in the scheelite, quartz, and calcite (Figure 6i).

As shown in Table 2, seventeen fluid inclusions of scheelite have been analyzed, and the ice temperatures are in the range of -4.2 to -1.8 °C. Homogenization temperatures of these inclusions mostly range from 220 to 297 °C. The salinities of these inclusions in scheelite range from 3.06 to 6.74 wt % NaCl equiv. For the quartz, the ice and homogenization temperatures of one hundred and eighty-six fluid inclusions range from -5.4 to -0.6 °C and from 175 to 290 °C, respectively, while the salinities of these inclusions of quartz range from 1.05 to 8.41 wt % NaCl equiv. In contrast to fluid inclusions of the syn-ore stage, calcite captures the fluid inclusions with higher ice temperatures but lower homogenization temperatures and salinities. In details, the ice temperatures of thirteen inclusions vary from -2.2 to -0.7 °C, while homogenization temperatures and salinities are from 145–218 °C and 1.23 to 3.71 wt % NaCl equiv.

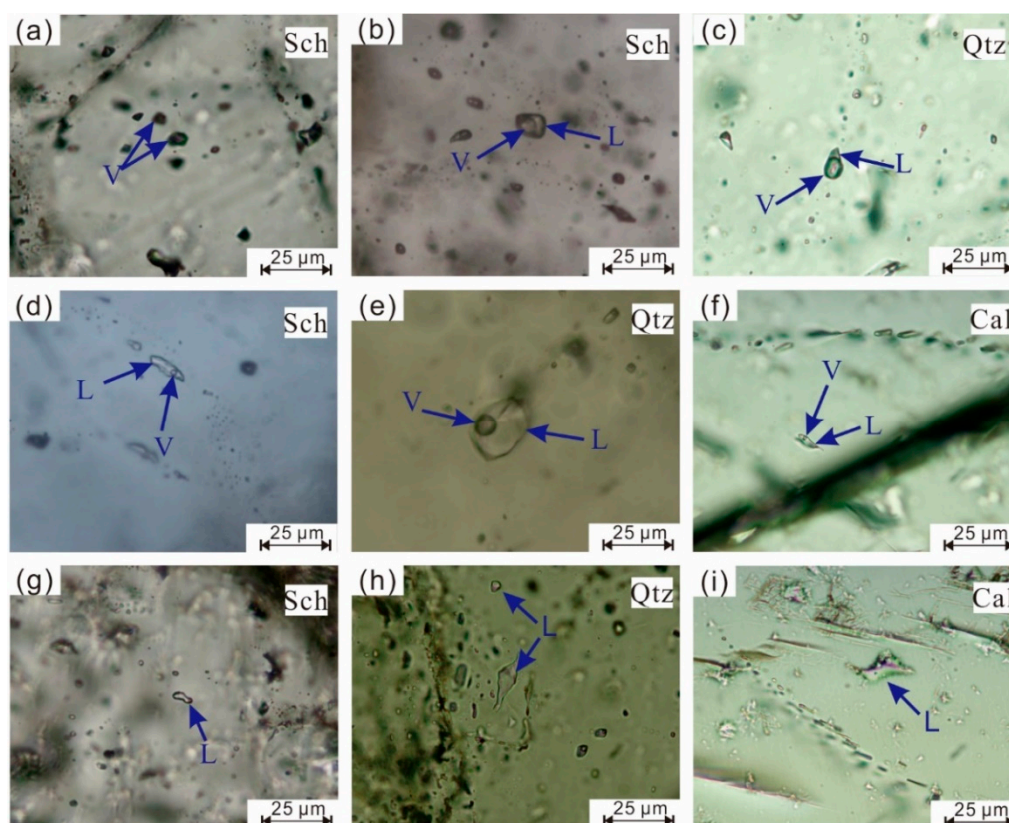


Figure 6. Photomicrograph of different fluid inclusions found in scheelite, quartz, and calcite from the Shangfang tungsten deposit. (a) monophase vapor (V) inclusions in scheelite; (b,c) aqueous liquid (L-V) inclusions in scheelite and quartz; (d–f) vapor-rich aqueous (V-L) inclusions in scheelite, quartz and calcite; (g–i) liquid aqueous (L) inclusions in scheelite, quartz, and calcite. Abbreviations: L = liquid; V = vapor; Sch = scheelite; Cal = calcite; Qtz = quartz.

Table 2. Summary of microthermometric measurements.

Stage	Mineral	T_h (°C)	T_{m-ice} (°C)	Salinity (wt % NaCl equiv.)
		Range	Range	Range
Syn-ore	Scheelite	220 to 297	−4.2 to −1.8	3.06 to 6.74
	Quartz	175 to 290	−5.4 to −0.6	1.05 to 8.41
Post-ore	Calcite	145 to 218	−2.2 to 0.7	1.23 to 3.71

5.2. Hydrogen and Oxygen Isotopic Compositions

The results about H–O isotopic composition of quartz are listed in Table 3. The $\delta^{18}O_{V-SMOW}$ values of quartz show a range from 11.3‰ to 12.3‰, whereas water of fluid inclusions trapped in quartz present δD values from −57.1‰ to −76.3‰. The $\delta^{18}O_{fluid}$ values are correlating to the temperature for calibration. Due to the absence of pressures estimation, the actual entrapment temperature may be far higher than the measured homogenization temperature under the atmospheric pressure. The oxygen isotopic compositions of hydrothermal water are calculated against estimated temperatures (400 °C, 350 °C, and 300 °C) that are higher than the measured homogenization temperature of fluid inclusions. In detail, the calculated $\delta^{18}O_{fluid}$ values respectively range from 6.74‰ to 7.74‰, from 5.50‰ to 6.50‰, and from 3.91‰ to 4.91‰, while the temperature was 400 °C, 350 °C, and 300 °C.

Table 3. Hydrogen and oxygen isotopic compositions of ore-bearing quartz from the Shangfang W deposit.

Sample Number	δD_{V-SMOW}	$\delta^{18}O_{V-SMOW}$	$\delta^{18}O_{H_2O}(\text{‰})$		
			T = 400 °C	T = 350 °C	T = 300 °C
SFI01	−67	12.1	7.54	6.30	4.71
SFI02	−57.1	12.3	7.74	6.50	4.91
SFI03	−63	11.3	6.74	5.50	3.91
SFI04	−64	11.7	7.14	5.90	4.31
SFI05	−76.3	11.7	7.14	5.90	4.31
SFI06	−61.4	11.9	7.34	6.10	4.51

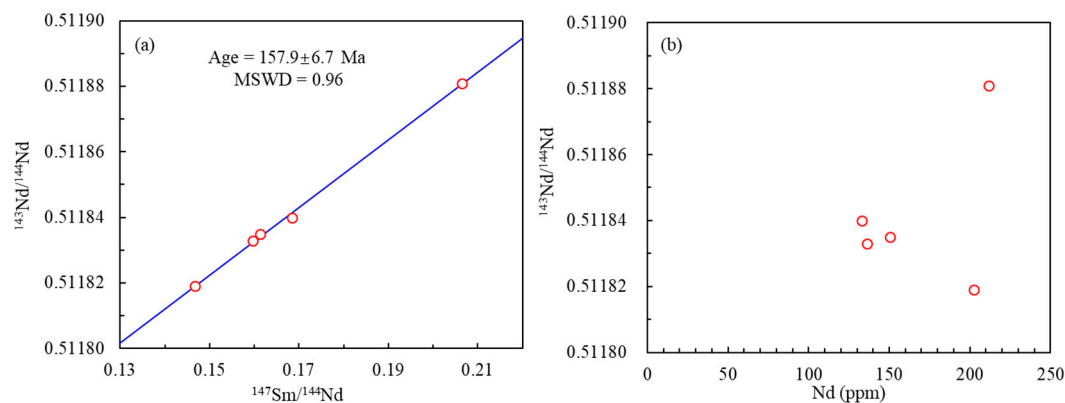
5.3. Sm-Nd Dating

Sm-Nd isotopic results of scheelite from the drill core are summarized in Table 4. The five scheelite samples that were used for Sm-Nd dating show slight variations in Sm (35.91 to 72.26 ppm) and Nd (132.9 to 211.7 ppm) concentrations. The Sm-Nd isochron age was calculated using the ISOPLOT plotting program [39]. In this study, the decay constant (λ) of the half-life for ^{147}Sm was $6.54 \times 10^{-12} \text{ a}^{-1}$, and the $^{147}\text{Sm}/^{144}\text{Nd}$ (0.1967) and $^{143}\text{Nd}/^{144}\text{Nd}$ values (0.512638) of the chondritic uniform reservoir (CHUR) were used for the $\epsilon_{\text{Nd}}(t)$ calculations, respectively. In general, the $^{147}\text{Sm}/^{144}\text{Nd}$ ratios and present $^{143}\text{Nd}/^{144}\text{Nd}$ ratios vary from 0.1467 to 0.2065 and 0.511819 to 0.511881, respectively, and yield a correlation line owing to the absence of any correlation in the $^{143}\text{Nd}/^{144}\text{Nd}$ vs. Nd diagram (Figure 7b). Hence, we can exclude the possibility of a mixing line. Thus an excellent isochron is obtained, yielding an age of $157.9 \pm 6.7 \text{ Ma}$ with an MSWD = 0.96 (Figure 7a). Moreover, the calculated $\epsilon_{\text{Nd}}(t)$ of scheelite show a range from −14.6 to −14.7 (Table 4). Given the similar molybdenite Re-Os isochron age of $158.1 \pm 5.4 \text{ Ma}$ and the zircon U-Pb age of $158.8 \pm 3.2 \text{ Ma}$, it is reasonable to interpret the Sm-Nd isochron age of $157.9 \pm 6.7 \text{ Ma}$ as an actual age of the tungsten mineralization in the Shangfang W deposit.

Table 4. Sm-Nd isotopic result of scheelite samples from the drill core of Shangfang tungsten deposit.

Sample	Sm (ppm)	Nd (ppm)	$^{147}\text{Sm}/^{144}\text{Nd}$	$^{143}\text{Nd}/^{144}\text{Nd}$	2σ	$^{143}\text{Nd}/^{144}\text{Nd}(t)$	$\epsilon_{\text{Nd}}(t)$
ZK001-4	49.14	202.6	0.1467	0.511819	± 2	0.511669	−14.6
ZK204-1	36.99	132.9	0.1684	0.511840	± 2	0.511668	−14.7
ZK204-2	35.91	136.1	0.1596	0.511833	± 2	0.511670	−14.6
ZK803-1	40.15	150.6	0.1613	0.511836	± 3	0.511670	−14.6
ZK1003-2	72.26	211.7	0.2065	0.511881	± 2	0.511670	−14.6

Note: the isochron age of scheelite (157.9 Ma), $(^{147}\text{Sm}/^{144}\text{Nd})_{\text{CHUR}} = 0.1967$ and $(^{143}\text{Nd}/^{144}\text{Nd})_{\text{CHUR}} = 0.512638$ are used to calculate the $\epsilon_{\text{Nd}}(t)$ values of scheelite.

**Figure 7.** (a) Sm-Nd isochron, and (b) the relationship between $^{143}\text{Nd}/^{144}\text{Nd}$ and Nd content obtained from scheelite of the Shangfang W deposit.

6. Discussion

6.1. Evolution of Ore-Forming Fluids

In the quartz and scheelite, most of the primary fluid inclusion include intermediate-low salinity (3.06–6.74 wt % NaCl equivalent), which is higher than that of inclusions in calcite (Figure 8). Meanwhile, the salinities of fluid inclusions of scheelite agree well with that of some quartz when the homogenization temperatures range from 220 to 300 °C (Figure 9). Since some massive scheelite occurred in the quartz vein, the scheelite and early-stage quartz may precipitate simultaneously when the fluid has a relative higher temperature and salinity. In Figures 8 and 9, both the homogenization temperature and salinity of inclusions in quartz are lower than that in scheelite, which thus suggests the precipitation peak of quartz is slightly later than that of scheelite. Depressurization usually happens when the fluid is boiling and accompanied with crypto-explosions and/or hydraulic fracturing [40–42]. However, on the basis of the geological features, petrographic study, and microthermometric data, we did not find any geological and fluid inclusion evidence of depressurization in the Shangfang W deposit. Hence, the fluid inclusions in scheelite or quartz generally display a more extensive variation range of salinity, which is suggestive of a near-isothermal (possibly poly-baric) mixing between two fluids of differing salinity. If there is a meteoric fluid (salinity close to zero) added into the fluid system, the salinities of fluid inclusions would be obviously decreasing. This is also not shown in the Shangfang W deposit. Because the W orebodies occur in the metamorphic amphibolite, the possibility indeed exists of metamorphic rock exchange with the magmatic fluid system. As Figures 8 and 9 show, temperature variation and salinity stabilization from the scheelite to the quartz deposition in the syn-ore stage is distinct. It clearly testifies for a cooling process, which may be critical during the syn-ore stage in the Shangfang W deposit. Similar variation also can be observed in the giant Dahutang W deposits [5]. The lower salinity and homogenization temperature of the calcite indicates its fluid inclusions should be captured after deposition of scheelite and quartz (Figure 9). Moreover, the variation of salinity and homogenization temperature in calcite also clearly testify for cooling of the system.

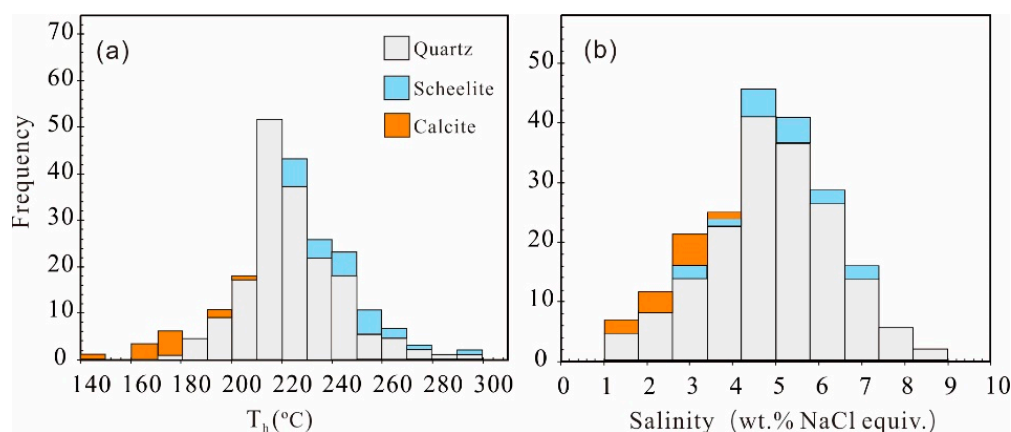


Figure 8. Histograms of (a) homogenization temperature and (b) salinity of the fluid inclusions in quartz, scheelite, and calcite.

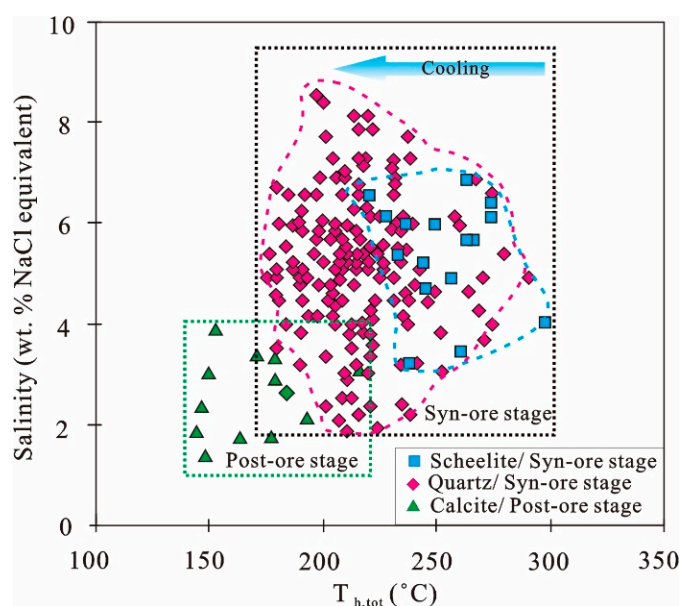


Figure 9. Covariation between homogenization temperature and salinity of fluid inclusions showing the evolution of the ore-forming fluids in the Shangfang W deposit.

6.2. Origin of Ore-Forming Fluids

It is acceptable that oxygen and hydrogen isotope compositions of hydrothermal quartz are useful for tracking the source of hydrothermal fluids. Given that the actual temperature of fluid inclusions (> -300 °C) is higher than the homogenization temperature under atmospheric conditions, the oxygen isotopic compositions are respectively calculated against 400, -350 , and -300 °C, as shown in Figure 10. The calculated results of oxygen and hydrogen isotope compositions in the Shangfang W deposit are all distributed in the variation range of ore fluids for polymetallic deposits in the coastal South China Block. When the temperature is higher than 300 °C, most of the $\delta^{18}\text{O}$ results are distributed within the area of primary magmatic water and the metamorphic water. The pieces of information from fluid inclusions have demonstrated the existence of a system involving different fluids for mineralization. In general, the salinity of fluid is in the range of metamorphic fluids (or of fluids equilibrated with metamorphic rocks at high temperature) rather than in that of actual magmatic fluids. Moreover, the coincidence among the results of the zircon U–Pb age (158.8 ± 1.6 Ma), molybdenite Re–Os age (158.1 ± 5.4 Ma), and Sm–Nd isochron age (157.9 ± 6.7 Ma) suggest that the granite magma should play a key role for mineralization. In summary, ore-forming fluids of the Shangfang W deposit might be derived from magma that exchanged with metamorphic water or equilibrated with metamorphic rocks at high T. There was a large (even crustal-scale) hydrothermal system, the heat for which would be advected by granite magmatism, to produce the large-scale W deposit in the Shangfang area.

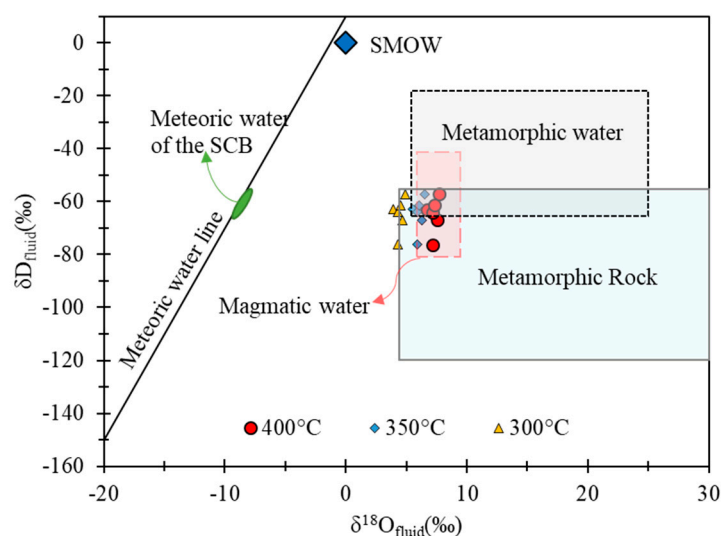


Figure 10. Hydrogen and oxygen isotope composition of quartz from the Shangfang W deposit. The range of Mesozoic meteoric water for the South China Block (SCB) is estimated according to previous works [43–45]. Furthermore, the H–O isotopic fields for ordinary metamorphic water is from Taylor [46], for primary magmatic water is from Hedenquist et al. [47], and for metamorphic rocks is from Hoefs et al. [48].

6.3. Place of the Shangfang Deposit in the Cathaysia Metallogenic Frame

It is widely admitted that three episodes of large-scale magmatic activity occurred in South China at Late Triassic (170–150 Ma), Mid-Late Jurassic (140–126 Ma), and Cretaceous (110–80 Ma) [3]. It is currently thought that these episodes coincide with large scale lithospheric delamination events related to the subduction of the Pacific Plate [22–24]. Generally, the episodes of magmatic activities are also roughly coincident with mineralization peaks of multi-metals (e.g., W–Sn, Fe, Cu, Pb–Zn, Ag and Au) during Yanshanian [2,19,49,50]. It produced a series of large, giant and super-giant tungsten deposits, defining three provinces in South China (Figure 11), including the Nanling Range Metallogenic Belt (e.g. Xihuashan, Huamei’ao, and Taoxikeng W–Sn deposits) [51–53], Southeastern Coastal Metallogenic Belt (e.g. Feie’shan, Lianhuashan, Xiling W–Sn deposits) [7,54,55] and Jiangnan porphyry–skarn W belt (e.g. Zhuxi and Dahutang W–Sn deposits) in the South China [6,19,21,56]. According to an increasing age data base, the Nanling Range was mainly formed during the Early Yanshanian (>150 Ma), whereas that of Southeastern Coastal Metallogenic Belt and Jiangnan porphyry–skarn W belt is slightly later (<150 Ma).

The Shangfang W deposit is located to the northeastern boundary of the Nanling Range Metallogenic Belt and the western boundary of the Southeastern Coastal Metallogenic Belt or on the contact of these metallogenic belts. The new-age data for the Shangfang deposit (157.9 ± 6.7 Ma) points to its affiliation to the Nanling Range Belt, to which also belongs another large-scale deposit in Fujian, the Xingluoking deposit dated at 156.3 ± 4.8 Ma [57]. Comparing with collected results of geochronology and locations information about W deposits in South China, it is evident that both mineralization backgrounds of the Shangfang and Xingluoking tungsten deposits agree well with that of tungsten deposits in the Nanling Range. The $\epsilon_{Nd}(t)$ of -14.6 obtained in the Shangfang scheelite testifies for the involvement of the deep crust, adding to the arguments linking the W belts to partial melting of the lower crust under the influence of the subducted paleo-Pacific plate [20,58].

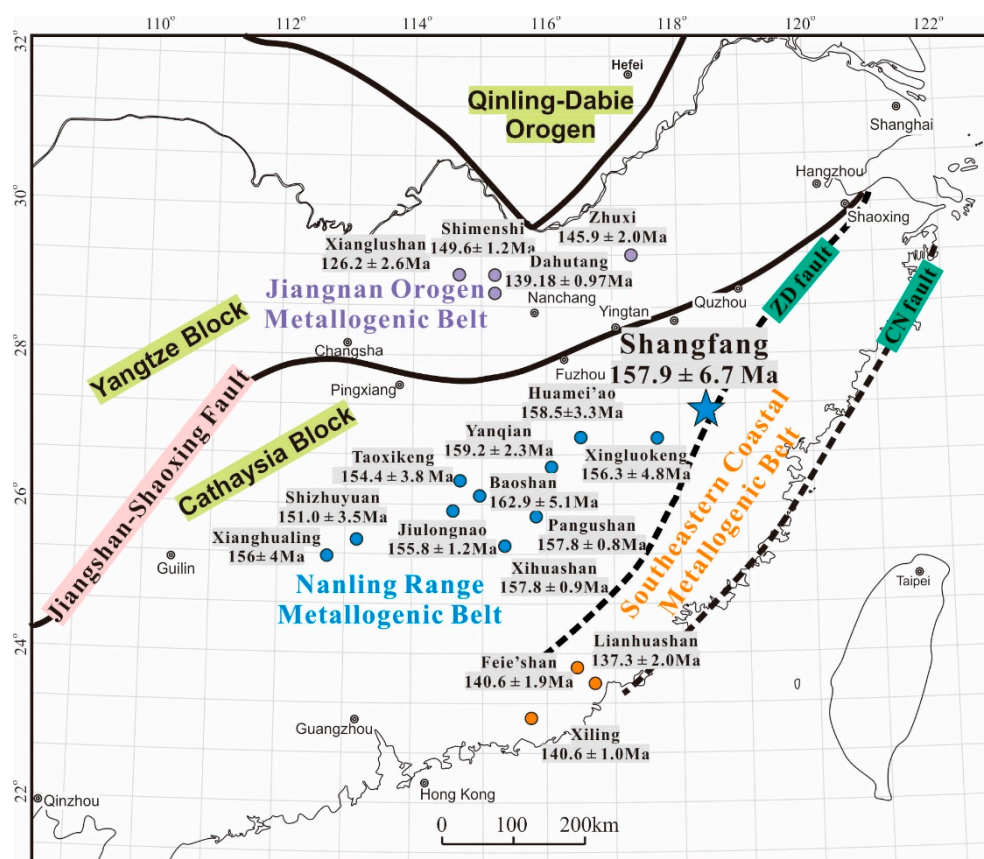


Figure 11. Simplified geological map of South China and distribution of some granite-related W-Sn deposits. ZD fault and CN fault are Zhenghe-Dapu Fault and Changle-Nan'ao Fault along the coastal area. The age database of three Metallogenic Belts is collected from previous works [7,51–68].

7. Conclusions

Although the orebody of Shangfang W deposit occurs in the Paleoproterozoic metamorphic amphibolite, it still shares many similar features with quartz-vein type W deposits worldwide. The Microthermometry results of fluid inclusions in scheelite and quartz is suggestive of a near-isothermal (possibly poly-baric) mixing between two fluids of differing salinities. The H–O isotopic compositions of quartz demonstrate that ore-forming fluids of the Shangfang W deposit are derived from magma and might be equilibrated with metamorphic rocks at high temperature. Because the Sm–Nd age of scheelite (157.9 ± 6.7 Ma) agree well with the zircon U–Pb age of the granite (158.8 ± 1.6 Ma) and Re–Os age (158.1 ± 5.4 Ma) of molybdenite, the Jurassic granite pluton should play a critical role for the large (even crustal-scale) hydrothermal system producing the Shangfang W deposit. In addition, the negative $\varepsilon_{\text{Nd}}(t)$ of -14.6 obtained in the Shanfang scheelite testifies for the involvement of the deep crustal materials. In general, subduction of the paleo-Pacific plate causes an extensional environment with formation of the Shangfang granites and related W deposit, and the geological background of which is similar to other W deposits in the Nanling Range Metallogenic Belt in south China.

Author Contributions: Conceptualization, L.-Y.Z. and S.-Y.J.; funding acquisition, S.-Y.J. and R.-S.C.; resources, L.-Y.Z. and R.-S.C.; investigation, L.-Y.Z. and R.-S.C.; methodology, L.-Y.Z. and Y.M.; formal analysis L.-Y.Z. and Y.M.; data curation, L.-Y.Z.; writing—original draft, L.-Y.Z.; writing—revision and editing, S.-Y.J. and L.-Y.Z.

Funding: This research was funded by the National Key R&D Program of China (2017YFC0602405), the National Natural Science Foundation of China (41803012), the China Postdoctoral Science Foundation (2017M622546), and the special fund from the State Key Laboratory of Geological Processes and Mineral Resources, China University of Geosciences (no. MSFGPMR03-2).

Acknowledgments: Special thanks should go to two anonymous reviewers who have given detailed suggestions and comments, which improved the quality of this manuscript. We highly appreciate the constructive comments of Kui-Dong Zhao and Suo-Fei Xiong regarding an earlier version of this manuscript. We are also grateful to Xi-Run Tong for the assistance of Sm-Nd dating.

Conflicts of Interest: The authors declare no conflict of interest. The funders had no role in the design of the study; in the collection, analyses, or interpretation of data; in the writing of the manuscript, or in the decision to publish the results.

References

1. Schulz, K.J.; DeYoung, J.H.; Seal, R.R.; Bradley, D.C. *Critical Mineral Resources of the United States: Economic and Environmental Geology and Prospects for Future Supply*; U.S. Geological Survey: Reston, VA, USA, 2018.
2. Mao, J.W.; Chen, M.H.; Yuan, S.D. Geological Characteristics of the Qinhang (or Shihang) Metallogenic Belt in South China and Spatial-Temporal Distribution Regularity of Mineral Deposits. *Acta Geol. Sin.* **2011**, *85*, 636–658.
3. Mao, J.W.; Xie, G.Q.; Li, X.F.; Zhang, C.Q.; Wang, Y.T. Mesozoic Large-scale Mineralization and Multiple Lithospheric Extensions in South China. *Acta Geol. Sin.* **2006**, *80*, 420–431.
4. Hua, R.M.; Chen, P.R.; Zhang, W.L.; Yao, J.M.; Lin, J.F.; Zhang, Z.S.; Gu, S.Y. Metallogenesis and Their Geodynamic Settings Related to Mesozoic Granitoids in the Nanling Range. *Geol. J. China Univ.* **2005**, *11*, 291–304.
5. Peng, N.J.; Jiang, S.Y.; Xiong, S.F.; Pi, D.H. Fluid evolution and ore genesis of the Dalingshang deposit, Dahutang W-Cu ore field, northern Jiangxi Province, South China. *Mineral. Depos.* **2018**, *53*, 1079–1094. [[CrossRef](#)]
6. Huang, L.C.; Jiang, S.Y. Highly fractionated S-type granites from the giant Dahutang tungsten deposit in Jiangnan Orogen, Southeast China: Geochronology, petrogenesis and their relationship with W-mineralization. *Lithos* **2014**, *202*, 207–226. [[CrossRef](#)]
7. Liu, P.; Mao, J.W.; Santosh, M.; Xu, L.G.; Zhang, R.Q.; Jia, L.H. The Xiling Sn deposit, eastern Guangdong Province, Southeast China: A new genetic model from ⁴⁰Ar/³⁹Ar muscovite and U-Pb cassiterite and zircon geochronology. *Econ. Geol.* **2018**, *113*, 511–530. [[CrossRef](#)]
8. Chen, R.S.; Li, J.W.; Cao, K.; Qu, C.Y.; Li, Y.J. Zircon U-Pb and Molybdenite Re-Os dating of the Shangfang Tungsten Deposit in Northern Fujian Province: Implication for Regional Mineralization. *J. China Univ. Geosci.* **2013**, *38*, 289–303.
9. Charvet, J. The Neoproterozoic–Early Paleozoic tectonic evolution of the South China Block: An overview. *J. Asian Earth Sci.* **2013**, *74*, 198–209. [[CrossRef](#)]
10. Zhao, J.H.; Zhou, M.F.; Yan, D.P.; Zheng, J.P.; Li, J.W. Reappraisal of the ages of Neoproterozoic strata in South China: No connection with the Grenvillian orogeny. *Geology* **2011**, *39*, 299–302. [[CrossRef](#)]
11. Li, X.H.; Li, W.X.; Li, Z.X.; Lo, C.H.; Wang, J.; Ye, M.F.; Yang, Y.H. Amalgamation between the Yangtze and Cathaysia Blocks in South China: Constraints from SHRIMP U–Pb zircon ages, geochemistry and Nd–Hf isotopes of the Shuangxiwu volcanic rocks. *Precambrian Res.* **2009**, *174*, 117–128. [[CrossRef](#)]
12. Ling, W.L.; Gao, S.; Zhang, B.R.; Li, H.M.; Liu, Y.; Cheng, J.P. Neoproterozoic tectonic evolution of the northwestern Yangtze craton, South China: Implications for amalgamation and break-up of the Rodinia Supercontinent. *Precambrian Res.* **2003**, *122*, 111–140. [[CrossRef](#)]
13. Yu, J.H.; O’Reilly, S.Y.; Zhou, M.F.; Griffin, W.L.; Wang, L.J. U–Pb geochronology and Hf–Nd isotopic geochemistry of the Badu Complex, Southeastern China: Implications for the Precambrian crustal evolution and paleogeography of the Cathaysia Block. *Precambrian Res.* **2012**, *222*, 424–449. [[CrossRef](#)]
14. Chen, J.F.; Foland, K.A.; Xing, F.M.; Xu, X.A.; Zhou, T.X. Magmatism Along The Southeast Margin Of The Yangtze Block—Precambrian Collision Of The Yangtze And Cathaysia Blocks Of China. *Geology* **1991**, *19*, 815–818.
15. Yu, J.H.; Zhou, X.M.; O’Reilly, Y.S.; Zhao, L.; Griffin, W.L.; Wang, R.C.; Wang, L.J.; Chen, X.M. Formation history and protolith characteristics of granulite facies metamorphic rock in Central Cathaysia deduced from U–Pb and Lu–Hf isotopic studies of single zircon grains. *Chin. Sci. Bull.* **2005**, *50*, 2080–2089. [[CrossRef](#)]
16. Wang, L.J.; Yu, J.H.; O’Reilly, S.Y.; Griffin, W.L.; Sun, T.; Wei, Z.Y.; Jiang, S.Y.; Shu, L.S. Grenvillian orogeny in the Southern Cathaysia Block: Constraints from U–Pb ages and Lu–Hf isotopes in zircon from metamorphic basement. *Chin. Sci. Bull.* **2008**, *53*, 3037–3050. [[CrossRef](#)]

17. Li, Y.J.; Wei, J.H.; Chen, H.Y.; Tan, J.; Fu, L.B.; Wu, G. Origin of the Maoduan Pb–Zn–Mo deposit, eastern Cathaysia Block, China: Geological, geochronological, geochemical, and Sr–Nd–Pb–S isotopic constraints. *Mineral. Depos.* **2012**, *47*, 763–780. [[CrossRef](#)]
18. Cai, Y.P.; Guo, X.P.; Xia, C.J.; Lü, S.B.; Yu, Y.C.; Wang, S.X. Element abundance of crust in Fujian Province. *Geol. Fujian* **1997**, *16*, 163–175.
19. Mao, Z.H.; Cheng, Y.B.; Liu, J.J.; Yuan, S.D.; Wu, S.H.; Xiang, X.K.; Luo, X.H. Geology and molybdenite Re–Os age of the Dahutang granite-related veinlets-disseminated tungsten ore field in the Jiangxin Province, China. *Ore Geol. Rev.* **2013**, *53*, 422–433. [[CrossRef](#)]
20. Zhao, W.W.; Zhou, M.F.; Li, Y.H.M.; Zhao, Z.; Gao, J.F. Genetic types, mineralization styles, and geodynamic settings of Mesozoic tungsten deposits in South China. *J. Asian Earth Sci.* **2017**, *137*, 109–140. [[CrossRef](#)]
21. Song, S.W.; Mao, J.W.; Zhu, Y.F.; Yao, Z.Y.; Chen, G.H.; Rao, J.F.; Ouyang, Y.P. Partial-melting of fertile metasedimentary rocks controlling the ore formation in the Jiangnan porphyry-skarn tungsten belt, south China: A case study at the giant Zhuxi W–Cu skarn deposit. *Lithos* **2018**, *304–307*, 180–199. [[CrossRef](#)]
22. Zhou, X.M.; Sun, T.; Shen, W.Z.; Shu, L.S.; Niu, Y.L. Petrogenesis of Mesozoic granitoids and volcanic rocks in South China: A response to tectonic evolution. *Episodes* **2006**, *29*, 26–33. [[CrossRef](#)]
23. Lei, L.; Xu, X.S.; Yan, X. Asynchronizing paleo-Pacific slab rollback beneath SE China: Insights from the episodic Late Mesozoic volcanism. *Gondwana Res.* **2015**, *37*, 397–407.
24. Xia, Y.; Xu, X.; Zou, H.; Liu, L. Early Paleozoic crust–mantle interaction and lithosphere delamination in South China Block: Evidence from geochronology, geochemistry, and Sr–Nd–Hf isotopes of granites. *Lithos* **2014**, *184–187*, 416–435. [[CrossRef](#)]
25. Zhou, X.M.; Li, W.X. Origin of Late Mesozoic igneous rocks in Southeastern China: Implications for lithosphere subduction and underplating of mafic magmas. *Tectonophysics* **2000**, *326*, 269–287. [[CrossRef](#)]
26. Sun, T.; Zhou, X.M.; Chen, P.R.; Li, H.M.; Zhou, H.Y.; Wang, Z.C.; Shen, W.Z. Strongly peraluminous granites of Mesozoic in Eastern Nanling Range, southern China: Petrogenesis and implications for tectonics. *Sci. China Ser. D* **2005**, *48*, 165–174. [[CrossRef](#)]
27. Li, Z.X.; Li, X.H. Formation of the 1300-km-wide intracontinental orogen and postorogenic magmatic province in Mesozoic South China: A flat-slab subduction model. *Geology* **2007**, *35*, 179–182. [[CrossRef](#)]
28. Wang, Y.J.; Fan, W.M.; Min, S.; Liang, X.Q.; Zhang, Y.H.; Peng, T.P. Geochronological, geochemical and geothermal constraints on petrogenesis of the Indosinian peraluminous granites in the South China Block: A case study in the Hunan Province. *Lithos* **2007**, *96*, 475–502. [[CrossRef](#)]
29. Hua, R.M.; Chen, P.R.; Zhang, W.L.; Lu, J.J. Three major metallogenic events in Mesozoic in South China. *Miner. Depos.* **2005**, *24*, 99–107.
30. Li, X.H.; Li, W.X.; Wang, X.C.; Li, Q.L.; Liu, Y.; Tang, G.Q. Role of mantle-derived magma in genesis of early Yanshanian granites in the Nanling Range, South China: In situ zircon Hf–O isotopic constraints. *Sci. China Ser. D* **2009**, *52*, 1262–1278. [[CrossRef](#)]
31. Li, Z.; Qiu, J.S.; Yang, X.M. A review of the geochronology and geochemistry of Late Yanshanian (Cretaceous) plutons along the Fujian coastal area of southeastern China: Implications for magma evolution related to slab break-off and rollback in the Cretaceous. *Earth Sci. Rev.* **2014**, *128*, 232–248. [[CrossRef](#)]
32. Li, Z.X.; Li, X.; Wartho, J.A.; Clark, C.; Li, W.; Zhang, C.L.; Bao, C.M. Magmatic and metamorphic events during the Early Paleozoic Wuyi-Yunkai orogeny, southeastern South China; New age constraints and pressure-temperature conditions. *Geol. Soc. Am. Bull.* **2010**, *122*, 772–793. [[CrossRef](#)]
33. Wan, Y.; Liu, D.; Xu, M.; Zhuang, J.; Song, B.; Shi, Y.; Du, L. SHRIMP U–Pb zircon geochronology and geochemistry of metavolcanic and metasedimentary rocks in Northwestern Fujian, Cathaysia block, China: Tectonic implications and the need to redefine lithostratigraphic units. *Gondwana Res.* **2007**, *12*, 166–183. [[CrossRef](#)]
34. Zhao, L.; Zhou, X.; Zhai, M.; Santosh, M.; Geng, Y. Zircon U–Th–Pb–Hf isotopes of the basement rocks in northeastern Cathaysia block, South China: Implications for Phanerozoic multiple metamorphic reworking of a Paleoproterozoic terrane. *Gondwana Res.* **2015**, *28*, 246–261. [[CrossRef](#)]
35. Mei, H.L.; Zhuang, J.M.; Yang, C.X. P–T–t paths and geodynamic implication of Precambrian metamorphic rocks in northern Fujian. *Geol. Fujian* **1993**, *12*, 182–194.
36. Zhao, G.C.; Cawood, P.A. Tectonothermal evolution of the Mayuan assemblage in the Cathaysia Block: Implications for neoproterozoic collision-related assembly of the South China craton. *Am. J. Sci.* **1999**, *299*, 309–339. [[CrossRef](#)]

37. Clayton, R.N.; Mayeda, T.K. The use of bromine pentafluoride in the extraction of oxygen from oxides and silicates for isotopic analysis. *Geochim. Cosmochim. Acta* **1963**, *27*, 43–52. [[CrossRef](#)]
38. Chu, Z.Y.; Guo, J.H.; Yang, Y.H.; Qi, L.; Chen, L.; Li, X.C.; Gao, J.F. Evaluation of sample dissolution method for Sm-Nd isotopic analysis of scheelite. *J. Anal. At. Spectrom.* **2012**, *27*, 509–515. [[CrossRef](#)]
39. Ludwig, K.R. User's manual for isoplot 3.00, a geochronological toolkit for microsoft excel. *Berkeley Geochronol. Cent. Spec. Publ.* **2003**, *4*, 25–32.
40. Roedder, E. Fluid inclusions. *Rev. Miner.* **1984**, *12*, 1–644.
41. Kreuzer, O.P. Intrusion-hosted mineralization in the Charters Towers Goldfield, North Queensland: New isotopic and fluid inclusion constraints on the timing and origin of the auriferous veins. *Econ. Geol.* **2005**, *100*, 1583–1603. [[CrossRef](#)]
42. Xiong, S.; He, M.; Yao, S.; Cui, Y.; Shi, G.; Ding, Z.; Hu, X. Fluid evolution of the Chalukou giant Mo deposit in the northern Great Xing'an Range, NE China. *Geol. J.* **2015**, *50*, 720–738. [[CrossRef](#)]
43. Zhang, L.G. *The Application of the Stable Isotope to Geology*; Shanxi Science and Technology Publishing House Xi'an: Shanxi, China, 1985; pp. 54–250.
44. Zhou, T.F.; Yue, S.C. Isotope geochemistry of copper mineralization in Yueshan, Anhui Province. *Miner. Depos.* **1996**, *4*, 341–350.
45. Xu, Y.M.; Jiang, S.Y.; Zhu, Z.Y.; Zhou, W. Mineral chemistry and H–O–S–Pb isotopic compositions of skarn type copper deposits in the Jiurui district of the Middle-Lower Yangtze River metallogenic belt, Eastern China. *Ore Geol. Rev.* **2015**, *69*, 88–103. [[CrossRef](#)]
46. Taylor, H.P. The application of oxygen and hydrogen isotope studies to problems of hydrothermal alteration and ore deposition. *Econ. Geol.* **1974**, *69*, 843–883. [[CrossRef](#)]
47. Hedenquist, J.W.; Lowenstern, J.B. The role of magmas in the formation of hydrothermal ore deposits. *Nature* **1994**, *370*, 519. [[CrossRef](#)]
48. Hoefs, J.; Hattori, K. Stable Isotope Geochemistry. *Sediment. Geol.* **1997**, *114*, 321.
49. Hu, R.Z.; Zhou, M.F. Multiple Mesozoic mineralization events in South China—an introduction to the thematic issue. *Miner. Depos.* **2012**, *47*, 579–588. [[CrossRef](#)]
50. Ma, Y.; Jiang, S.Y.; Chen, R.S.; Li, X.X.; Zhu, L.Y.; Xiong, S.F. Hydrothermal evolution and ore genesis of the Zhaiping Ag–Pb–Zn deposit in Fujian Province of Southeast China: Evidence from stable isotopes (H, O, C, S) and fluid inclusions. *Ore Geol. Rev.* **2019**, *104*, 246–265. [[CrossRef](#)]
51. Feng, C.Y.; Zhao, Z.; Qu, W.J.; Zeng, Z.L. Temporal consistency between granite evolution and tungsten mineralization in Huamei'ao, southern Jiangxi Province, China: Evidence from precise zircon U–Pb, molybdenite Re–Os, and muscovite 40Ar – 39Ar isotope geochronology. *Ore Geol. Rev.* **2015**, *65*, 1005–1020. [[CrossRef](#)]
52. Hu, R.Z.; Wei, W.F.; Bi, X.W.; Peng, J.T.; Qi, Y.Q.; Wu, L.Y.; Chen, Y.W. Molybdenite Re–Os and muscovite $40\text{Ar}/39\text{Ar}$ dating of the Xihuashan tungsten deposit, central Nanling district, South China. *Lithos* **2012**, *150*, 111–118. [[CrossRef](#)]
53. Chen, Z.H.; Wang, D.H.; Qu, W.J.; Chen, Y.C.; Wang, P.A.; Xu, J.X.; Zhang, J.J. Geological characteristics and mineralization age of the Taoxikeng tungsten deposit in Chongyi County, southern Jiangxi Province, China. *Geol. Bull. China* **2006**, *25*, 496–501.
54. Liu, P.; Mao, J.W.; Pirajno, F.; Jia, L.H.; Zhang, F.; Li, Y. Ore genesis and geodynamic setting of the Lianhuashan porphyry tungsten deposit, eastern Guangdong Province, SE China: Constraints from muscovite 40Ar – 39Ar and zircon U–Pb dating and Hf isotopes. *Miner. Depos.* **2018**, *53*, 797–814. [[CrossRef](#)]
55. Liu, P.; Mao, J.W.; Cheng, Y.B.; Yao, W.; Wang, X.Y.; Hao, D. An Early Cretaceous W–Sn deposit and its implications in southeast coastal metallogenic belt: Constraints from U–Pb, Re–Os, Ar–Ar geochronology at the Feie'shan W–Sn deposit, SE China. *Ore Geol. Rev.* **2017**, *81*, 112–122. [[CrossRef](#)]
56. Pan, X.F.; Hou, Z.Q.; Li, Y.; Chen, G.H.; Zhao, M.; Zhang, T.F.; Zhang, C.; Wei, J.; Kang, C. Dating the giant Zhuxi W–Cu deposit (Taqian–Fuchun Ore Belt) in South China using molybdenite Re–Os and muscovite Ar–Ar system. *Ore Geol. Rev.* **2017**, *86*, 719–733. [[CrossRef](#)]
57. Zhang, J.J.; Chen, Z.H.; Wang, D.H.; Chen, Z.Y.; Liu, S.B.; Wang, C.H. Geological characteristics and metallogenic epoch of the Xingluokeng tungsten deposit, Fujian Province. *Geotecton. Metallog.* **2008**, *32*, 92–97.
58. Zhou, M.F.; Gao, J.F.; Zhao, Z.; Zhao, W.W. Introduction to the special issue of Mesozoic W–Sn deposits in South China. *Ore Geol. Rev.* **2018**, *101*, 432–436. [[CrossRef](#)]

59. Liu, P.; Cheng, Y.B.; Wang, X.Y.; Zhang, X.; Gao, F.Y.; Liao, Z.G. Zircon U-Pb geochronology and characteristics of Hf isotope from the Taoziwo Sn deposit in eastern Guangdong Province and their significance. *Acta Petrol. Miner.* **2015**, *34*, 620–636.
60. Zhao, J.H.; Zhou, M.F.; Zheng, J.P. Constraints from zircon U–Pb ages, O and Hf isotopic compositions on the origin of Neoproterozoic peraluminous granitoids from the Jiangnan Fold Belt, South China. *Contrib. Miner. Petrol.* **2013**, *166*, 1505–1519. [[CrossRef](#)]
61. Zeng, Z.L.; Zhang, Y.Z.; Chen, Z.H.; Chen, Y.C.; Zhu, X.P.; Tong, Q.Q.; Zheng, B.H.; Zhou, Y. Geological characteristics and metallogenic epoch of Pangushan W-Bi (Te) ore deposit in Yudu County, Jiangxi province. *Miner. Depos.* **2011**, *30*, 949–958.
62. Feng, C.Y.; Fan, H.; Zeng, Z.L.; Qu, W.J. Isotopic Chronology of Jiulongnao Granite and Hongshuizhai Greisens-Type Tungsten Deposit in South Jiangxi Province. *J. Jilin Univ.* **2011**, *41*, 111–121.
63. Feng, C.Y.; Zhang, D.Q. Chronology of the Tungsten Deposits in Southern Jiangxi Province, and Episodes and Zonation of the Regional W-Sn Mineralization-Evidence from High-precision Zircon U-Pb, Molybdenite Re-Os and Muscovite Ar-Ar Ages. *Acta Geol. Sin.* **2012**, *86*, 555–567.
64. Feng, C.Y.; Zeng, Z.L.; Wang, S.; Liang, J.S.; Ding, M. SHRIMP zircon U-Pb and Molybdenite Re-Os dating of the Skarn-type tungsten deposits in Southern Jiangxi province, China, and geological implications: Exemplified by the Jiaoli and Baoshan tungsten polymetallic deposits. *Geotecton. Metallog.* **2012**, *36*, 337–349.
65. Li, H.Y.; Mao, J.W.; Sun, Y.L.; Zou, X.Q.; He, H.L.; Du, A.D. Re-Os isotopic chronology of molybdenites in the Shizhuyuan polymetallic tungsten deposit, southern Hunan. *Geol. Rev.* **1996**, *42*, 261–267.
66. Yuan, S.D.; Peng, J.T.; Hu, R.Z.; Li, H.M.; Shen, N.P.; Zhang, D.L. A precise U–Pb age on cassiterite from the Xianghualing tin-polymetallic deposit (Hunan, South China). *Miner. Depos.* **2008**, *43*, 375–382. [[CrossRef](#)]
67. Feng, C.Y.; Zhang, D.Q.; Xiang, X.K.; Li, D.X.; Qu, H.Y.; Liu, J.N.; Xiao, Y. Re-Os isotopic dating of molybdenite from the Dahutang tungsten deposit in northwestern Jiangxi Province and its geological implication. *Acta Petrol. Sin.* **2012**, *28*, 3858–3868.
68. Zhang, J.J.; Mei, Y.P.; Wang, D.H.; Li, H.Q. Isochronology study on the Xianglushan Scheelite Deposit in North Jiangxi Province and its geological significance. *Acta Geol. Sin.* **2008**, *82*, 927–931.



© 2019 by the authors. Licensee MDPI, Basel, Switzerland. This article is an open access article distributed under the terms and conditions of the Creative Commons Attribution (CC BY) license (<http://creativecommons.org/licenses/by/4.0/>).